

Tu SRS3 07

Ultra-low Frequency Phase Assessment for Broadband Data

F. Yang* (CGG), R. Sablon (CGG) & R. Soubaras (CGG)

SUMMARY

Reliable low frequency content and phase alignment are critical for broadband seismic inversion and the prediction of reservoir properties. However, currently there is a lack of tools for ultra-low frequency (less than 5 Hz) quality and phase assessment. A focusing metric in the impedance domain is proposed to assess the ultra-low frequency phase alignment. The method has been applied on a real broadband dataset for the assessment of the residual phase correction process and the conclusion is validated by using well information.

Introduction

Phase alignment of the low frequencies is critical for broadband seismic inversion and the prediction of reservoir properties (Dennis *et al.*, 2000). However, there are several challenges for the ultra-low frequency phase assessment, including: (1) visual inspection of the ultra-low frequency phase on a seismic reflectivity section is subjective and inconclusive; (2) the length of the well logs is very often inadequate to measure the ultra-low frequency phase through a well tie. In this paper, we propose a solution by introducing a focusing metric in the impedance domain to evaluate the phase alignment for the ultra-low frequencies.

Method

The earth's reflectivity has a "blue" spectrum (Ulrych, 1999). In addition, the recorded seismic data is coloured by a band-limited wavelet whose amplitude spectrum drops sharply to zero as frequency tends toward to zero. Therefore, the response of ultra-low frequencies below 5 Hz is hardly visible on seismic images. To address this challenge, we transfer the seismic reflectivity to the impedance domain by integration, thus enhancing the low end significantly. Furthermore, seismic impedance is a layer property which is more closely related to geological interpretation and reservoir characterization than seismic reflectivity, which is related to impedance contrasts at geological interfaces.

Let $r(t)$ represent the earth reflectivity time series and $I_p(t)$ represent the acoustic impedance, the following relation holds: $\ln(I(t)) = 2 \int_0^t r(t') dt'$, where $I(t) \equiv I_p(t) - I_p(0)$ and $I_p(0)$ is the impedance at

time zero. If we replace $r(t)$ by the seismic trace $s(t) = r(t) * w(t) + n(t)$, where $w(t)$ is the seismic wavelet and $n(t)$ represents the noise term, and use the integration property of the Fourier transform, we obtain: $\mathcal{F}(\ln(I_{pse}(t))) = \frac{R(f)W(f) + N(f)}{i\pi f}$, where $I_{pse}(t)$ stands for the pseudo-impedance, f is the

frequency, $R(f)$, $W(f)$, and $N(f)$ are the Fourier transforms of $r(t)$, $w(t)$, and $n(t)$, respectively. Due to the band-limited character of the seismic wavelet $w(t)$ with an analogue low-cut in recording system and finite trace length, the singularity issue (when f is approaching zero frequency) does not exist in real data (Yilmaz, 2001).

The visual QC of the ultra-low frequencies alignment becomes possible on a pseudo-impedance section as a focused image can be obtained only when the ultra-low frequencies are properly aligned. For instance, any phase misalignments are reflected by the presence of precursor or tail around the inclusions (Figure 1a). After phase correction, the inclusions stand out from the background (Figure 1b). The amplitude spectra are rigorously identical in Figure 1a and 1b; improved imaging of the inclusions solely comes from phase alignment.

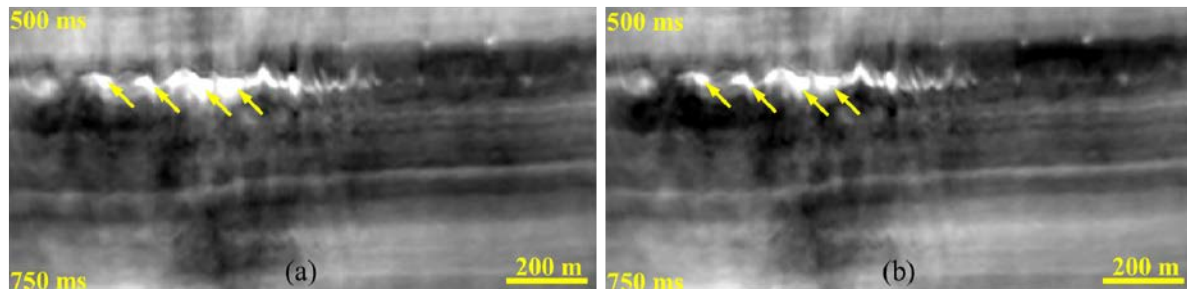


Figure 1 Logarithm of pseudo-impedance images (shallow water North-Sea data) showing inclusions: (a) ultra-low frequencies are not aligned; (b) ultra-low frequencies are aligned.

To quantify the focusing improvement upon phase alignment, inspired by the autofocus systems in machine vision, we propose the sum-modified-Laplacian focusing metric F (Nayar and Nakagawa, 1994) on the pseudo-impedance images to assess the ultra-low frequency phase alignment:

$$F(step, \Omega) = \frac{1}{N} * \frac{1}{RMS} * \sum_{(x,t) \in \Omega} \left| -I_{pse}(x, t - step) + 2 * I_{pse}(x, t) - I_{pse}(x, t + step) \right| + \left| -I_{pse}(x - step, t) + 2 * I_{pse}(x, t) - I_{pse}(x + step, t) \right|$$

where N is the number of samples and RMS stands for the rms average amplitude in the evaluation region Ω of the pseudo-impedance image $I_{pse}(x,t)$, x is the coordinate of the lateral direction, t is the coordinate in the depth direction, and $step$ is the spacing parameter to compute the second-order derivative. The value of F depends on the contrast of the pseudo-impedance. The higher the contrast is, the better the phase alignment, and the greater the value of F . The $step$ parameter can be adjusted to accommodate various size of geological texture (Nayar and Nakagawa, 1994). On various broadband datasets sampled at 2 ms along depth direction and 6 meters laterally, we have found that a step between 1 and 6 samples seems appropriate. We shall demonstrate the use of this metric on the pseudo-impedance images to assess the ultra-low frequency phase alignment.

Real data application

A conventional flat streamer and a variable-depth streamer (Soubaras and Dowle, 2010) were towed simultaneously in a seismic survey in 2011 in the North West Australia Shelf. The flat streamer was set at 7 meters below the sea surface while the variable-depth streamer ranged from 7 to 57 meters. An identical broadband processing sequence (denoising, designature, deghosting, demultiple and pre-stack time migration) has been applied to both data with pre-migration deghosting using a bootstrap approach in the tau-p domain (Wang *et al.*, 2013).

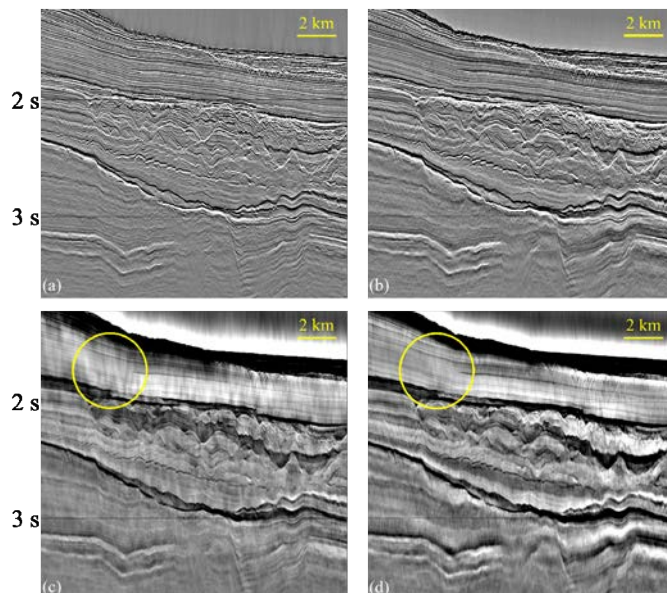


Figure 2 (a) seismic section of conventional flat streamer data with broadband processing; (b) seismic section of variable-depth streamer data; (c) logarithm of pseudo-impedance section for conventional flat streamer data with broadband processing; (d) logarithm of pseudo-impedance section for variable-depth streamer data. An example of low frequency noise is circled in (c) and (d).

In this case, where the acquisition noise level is very low, the final reflectivity image is quite similar between the broadband processed flat tow data and the variable-depth streamer data (Figure 2a and 2b). This is due to the fact that, in the seismic reflectivity section, the ultra-low frequency portion of the signal is barely visible except after a harsh 10 Hz high-cut filter. However, by converting the seismic to pseudo-impedance sections (Figure 2c and 2d), it is clear that the data acquired by variable-depth streamer offers a better signal quality at ultra-low frequencies with much less cross-hatched low-frequency noise. As a result the section has a better layer differentiation and continuity.

During the processing, a modelled far-field signature had been used for the designature process, which typically leaves a residual phase error in the seismic wavelet of the final section. The residual phase error can be estimated with either a conventional well-tie using a sonic log (Hampson and Galbraith, 1981) or a statistical data-driven blind deconvolution method (Yang *et al.*, 2015).

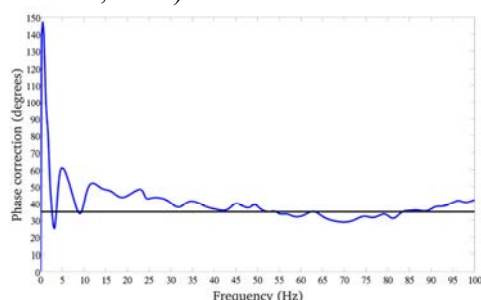


Figure 3 Frequency dependent phase correction (blue curve) obtained from blind deconvolution. The black straight line is the 35° constant phase correction derived from conventional seismic-to-well tie method.

Using available well information, we performed a conventional well-tie with a frequency independent sonic-log correlation method. An average of -35° phase error in the seismic wavelet is estimated from the broadband data shown in Figure 2b. Alternatively, a frequency-dependent phase error is estimated by statistical blind deconvolution (Yang *et al.*, 2015). Figure 3 shows the discrepancy between the phase corrections obtained by the two approaches. The statistical method indicates that the phase of the seismic data is highly unstable in the low frequency range, which is observed quite commonly on real broadband data and is caused by the air-gun bubbles.

We apply both these corrections independently to the data and perform seismic-to-well cross-correlation QC using a fixed zero-phase wavelet. Figure 4 shows the cross-correlation curves for various datasets: raw data, after constant phase correction and after frequency dependent phase correction. If the seismic data is zero-phase, the cross-correlation curve should be symmetric.

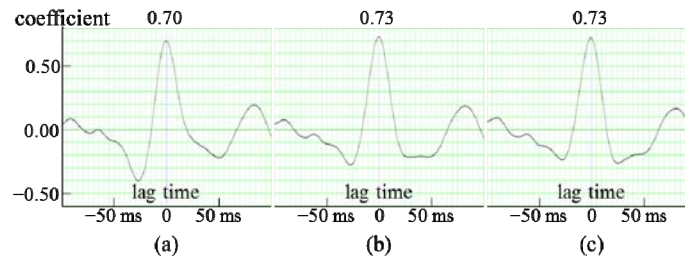


Figure 4 Seismic-to-well cross-correlation curves obtained (a) for raw input seismic; (b) after constant phase correction of 35° ; (c) after frequency dependent phase correction.

A close examination of the result reveals that the frequency dependent phase correction (Figure 4c) provides a more symmetrical cross-correlation curve, i.e., better zero-phasing. To further justify this, we apply focusing metric QC to benchmark these two approaches.

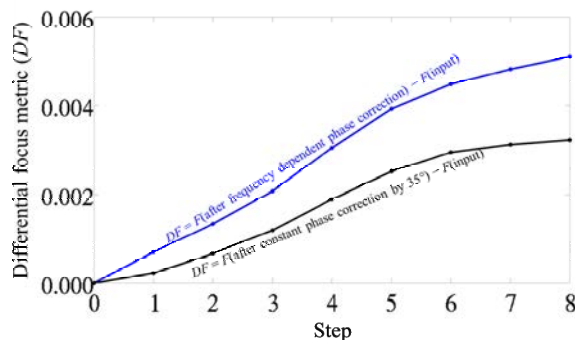


Figure 5 Differential focusing metric (DF) for data with frequency dependent phase correction (blue) and constant phase correction (black), under various parameterization of step size in samples.

We calculate the focusing metric F in the pseudo-impedance domain around the well location for various step sizes. For easier comparison, we compute the difference of the focusing metric F between the original pseudo-impedance and the pseudo-impedance after phase correction, namely differential focusing metric (DF). The result is also calculated for various step sizes. The DF curves shown in Figure 5 are positive for both approaches, thus indicating better phase alignment after the corrections. They also allow us to conclude that the frequency dependent phase correction yields better alignment than the constant $+35^\circ$ phase rotation. Even though the conclusion is independent of the step size, it is more obvious with larger step size up to 6 samples.

To further validate the conclusion, we carried out a post-stack acoustic inversion (Russell and Hampson, 1991) using a 2 Hz low frequency background velocity model (black line on the left “impedance” panels of Figure 6) and a fixed zero-phase statistical wavelet extracted from the seismic data. Two types of error indicator validate the inversions quality: (1) the impedance error (difference between the real well log impedances and the inversion impedances) and (2) the trace residue error (difference between the seismic trace and the synthetic trace created by the inverted impedance and the wavelet). Figure 6 shows that the prediction drawn from the differential focusing metric is verified by the well logs: a frequency dependent phase correction yields a better seismic inversion result (Figure 6c).

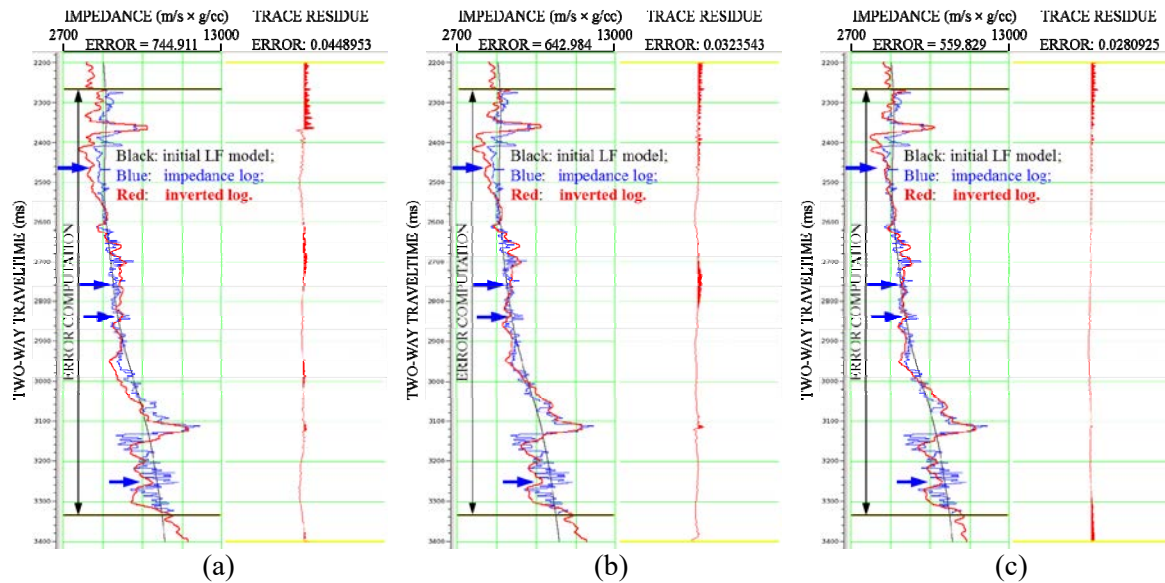


Figure 6 Inversion results: (a) for raw input seismic; (b) after constant phase correction of 35°; (c) after frequency dependent phase correction.

Conclusions

A focusing metric in the pseudo-impedance domain has been introduced to help assess the phase alignment of ultra-low frequency in broadband data. The method is applied on a real broadband dataset for assessing residual phase correction process and the conclusion drawn from this pure data-driven approach is validated by well information. Aided by the reliable low frequency signal content acquired by variable-depth streamer and frequency dependent low frequency phase alignment, seismic inversion can be performed adequately using data down to 2 Hz.

Acknowledgements

The authors gratefully acknowledge valuable help from Loic Michel for seismic inversion and fruitful discussions with Chu-Ong Ting and Richard Wombell on the properties of the focusing metric. We thank Lundin for the permission to show its North-Sea data.

References

- Dennis, L.P., Peterson, F.M., and Todorov, T.I. [2000] Inversion – the importance of low frequency phase alignment. *70th Annual International Meeting, SEG, Expanded Abstracts*, 1583-1586.
- Hampson, D. and Galbraith, M. [1981] Wavelet extraction by sonic-log correlation. *Journal of the Canadian Society of Exploration Geophysicists*, **17**, 24-42.
- Nayar, S.K. and Nakagawa, Y. [1994] Shape from focus. *IEEE Transactions on Pattern Analysis and Machine Intelligence*, **16**(8), 824-831.
- Russell, B. and Hampson, D. [1991] Comparison of post-stack seismic inversion methods. *61st Annual International Meeting, SEG, Expanded Abstracts*, 876-878.
- Soubaras, R. and Dowle, R. [2010] Variable-depth streamer - A broadband marine solution. *First Break*, **28**(12), 89-96.
- Ulrych, T.J. [1999] The whiteness hypothesis: Reflectivity, inversion, chaos, and Enders. *Geophysics*, **64**(5), 1512-1523.
- Wang, P., Ray, S., Peng, C., Yi, L. and Poole, G. [2013] Premigration deghosting for marine streamer data using a bootstrap approach in tau-p domain. *75th EAGE Conference and Exhibition, Extended Abstracts*.
- Yang, F., Sablon, R., and Soubaras, R. [2015] Time variant amplitude and phase dispersion correction for broadband data. *85th Annual International Meeting, SEG, Expanded Abstracts*, 4620-4625.
- Yilmaz, Ö. [2001] Seismic Data Analysis. *Investigations in Geophysics*, Society of Exploration Geophysicists, **10**, 2027.